Enhanced Young's Modulus of Al–Si Alloys and Reinforced Matrices by Co-continuous Structures

FERNANDO LASAGNI*,** AND HANS PETER DEGISCHER
Institute of Materials Science and Technology, Vienna University of Technology
Karlsplatz 13/E308, A-1040 Vienna, Austria

ABSTRACT: In the present work, the elastic behavior of different hypoeutectic and hypereutectic Al–Si alloys and different Al_2O_3 short fiber and SiC particle reinforced materials (SFRM and PRM, respectively) is studied. The effective Young's modulus (E) of materials was experimentally measured and compared with the different theoretical predictions of Hashin–Strikman, Tuchiniskii, shear lag, and the rule of mixtures (ROM). The unreinforced alloys present an interconnected lamellar Si structure after fast solidification, which increases the Young's modulus up to that of the Tuchiniskii prediction for interpenetrating skeletal structures. On the other hand, alloys presenting isolated and coarse Si particles (after spheroidization treatment at 540°C) are well described by the lower bound of the ROMs. Similarly, the interconnected Si–SiC structure observed in 10 and 70 vol% SiC reinforced AlSi7Mg and AlSi7 matrices in the as cast condition is responsible for the higher stiffness of the composite, if compared with that of Al99.5 or spheroidized AlSi7 matrices. An analogous behavior is observed in the SFRMs in the as cast condition, where the Si lamellae bridge the Al_2O_3 fibers, increasing the Young's modulus of the composites, if compared with the conditions of spheroidized Si. Furthermore, the primary Si particles produce an improvement in the Young's modulus by connecting several fibers in the case of a short fiber-reinforced hypereutectic AlSi18 matrix.

KEY WORDS: Al–Si alloys, metal matrix composites (MMCs), Interpenetrating Si network, Young's modulus, theoretical estimations.

INTRODUCTION

THE EXCELLENT CASTABILITY and mechanical properties of Al–Si alloys make them popular foundry alloys. The morphology of these alloys depends strongly on the Si content as well as on the casting process. As cast hypoeutectic alloys contain dendritic primary α-phase with an interpenetrating eutectic structure in between and between the

*Author to whom correspondence should be addressed. E-mail: flasagni@catec.aero
**Current address: FADA-CATEC, C/Wilbur y Orville Wright, 17-19-21, 41309 La Rinconada – Seville, Spain.

0021-9983/10/06 0739–17 $10.00/0 DOI: 10.1177/0021998309347649

secondary dendrite arms. The Si solidifies as an interpenetrating network [1,2] of thin (~1–2 μm) lamellae within the inter-dendritic spaces. Solution treatment of alloys containing more than 2 wt% Si produces the spheroidization of the eutectically solidified Si, improving the ductility of the alloys.

Aluminum Matrix Composites are considered for use in highly demanding automotive engines because of enhanced specific strength and stiffness at elevated temperatures provided by the ceramic reinforcement and some toughness by the Al-alloys [3–5]. Continuous structures of rigid phases enhance the stiffness of composites, if compared with discontinuously reinforced structures [6–8]. Stiffness is the main design criterion for structural components; increasing specific stiffness by interpenetrating structures allows a reduction in weight. Several researchers have conducted work in order to investigate the effect of the reinforcement connectivity in co-continuous structures: Peng et al. [9] reports on manufacturing and Young's modulus (E) estimation of infiltrated reticulated alumina preforms. For a given ceramic volume fraction, these composites possess higher Young's modulus than that of metal matrix composites (MMCs) with homogeneous reinforcement distribution [9,10]. In [11] a complete investigation of the experimental and modeled Young's modulus of several Al-interpenetrating composites is presented. Particularly, it is observed for the case of an AlSi12 alloy reinforced by 5–40% of an Al_2O_3 continuous preform a good correlation with Tuchinskii model [12] for interpenetrating structures (see section 'Tuchinskii Model'). Unfortunately, the effect of Si connectivity was not specifically studied. In [13] an interesting approach for predicting the elastic properties of interpenetrating multiphase composites is presented.

The objective of the present work is to investigate the effect of connectivity on the effective Young's modulus of several Al–Si alloys in the range 0–18 wt% Si, as well as in several particle and short fiber-reinforced AlSi matrices. The experimental results are compared with numerous analytical models based on different microstructural architectures. The role of the Si morphology is analyzed and related to the elastic behavior of these materials.

EXPERIMENTAL METHODS

Material Preparation

Three different types of materials were used in this work: AlSi-alloys; Al_2O_3 short fiber-reinforced materials (SFRMs), and SiC particle reinforced materials (PRMs). The AlSi-alloys were produced using a squeeze casting process by ARC–Leichtmetall Kompetenzzentrum Ranshofen (LKR), Austria. The Si content of the matrices was adjusted to AlSi1, a hypoeutectic AlSi7 alloy, a near eutectic AlSi12 and a hypereutectic AlSi18 alloy. 20 vol% Al_2O_3 preforms (produced by Thermal Ceramics de France S.A.) were infiltrated with the different matrices to produce four different SFRMs, hereafter designated as AlSiX/Al_2O_3/20s. Two AlSi7Mg and Al99.5 matrices were reinforced with 70 vol% SiC particles using a gas pressure infiltration method (by Electrovac GmbH, Kloesterneuburg, Austria) to produce two PRMs Al99.5/SiC/70p and AlSi7Mg/SiC/70p, respectively. The particle preforms were prepared from three modal powder sizes of average 80 μm (55 vol%), 20 and 5 μm (some details on fabrication process are given in [14]). The chemical composition of the alloys and matrices (provided by materials suppliers) is depicted in Table 1. A 10 vol% SiC particle reinforced AlSi7 alloy (AlSi7/SiC/10p) was

Table 1. Composition of the studied alloys and composites (Al-balance).

Matrix	Si (wt%)	Mg (wt%)	Fe (wt%)	MMC
Al99.5	<0.3	<0.01	<0.4	Al99.5/SiC/70p
AlSi1	1.11	<0.01	0.09	AlSi1.1/Al_2O_3/20s
AlSi7	7.04	<0.01	0.07	AlSi7/Al_2O_3/20s AlSi7/SiC/10p
AlSi7Mg	6.5–7.5	0.3–0.45	0.18	AlSi7Mg/SiC/70p
AlSi12	11.87	<0.01	0.08	AlSi12/Al_2O_3/20s
AlSi18	17.86	<0.01	0.16	AlSi18/Al_2O_3/20s

produced by stir casting at the *Instituto Universitario de Materiales de Alicante* of the Alicante University. For all materials, the reinforcement volume fraction was estimated by density measurements or metallographic determinations.

Samples of the AlSi-alloys, the SFRMs, and AlSi7/SiC/10p were solution treated (ST) at 540°C for 4 h (or 80 min in AlSi7/SiC/10p) using a Linn High Therm furnace 70.26 in order to spheroidize the eutectic Si-phase, and consecutively slowly cooled in air. The AlSi7Mg/SiC/70p composite was tested in the overaged condition (180°C/ >10 h) to avoid the age hardening effect of Mg_2Si precipitates.

Imaging of Percolating Networks

Small samples ($4 \times 4 \times 10\,mm^3$) of the unreinforced AlSi alloys in the as cast condition and composite materials in the as cast condition and after ST treatment were leached using 17 wt% HCl (during 48 h) to remove the Al-phase. A Si porous structure could be conserved from the AlSi7, AlSi12, and AlSi18 alloys in the as cast condition, while the ST samples disintegrated during chemical etching. A self-supporting Si–Al_2O_3 (SFRMs) and Si–SiC (PRMs) structure was extracted from the SFRMs with the as-cast alloy matrices and the PRMs, as well as from the SFRMs with the matrices in the ST condition. The extracted 3D networks were investigated using a FEI strata DB 235 electron microscope.

Young's Modulus Measurement

The Young's modulus E of the unreinforced AlSi alloys and composite materials was measured by means of a TA Instruments DMA 2980^{TM} dynamic mechanical analyzer using samples of $2 \times 4 \times 55\,mm^3$ size. Here, the sample's natural frequency of vibration was used to obtain the Young's modulus. The specimen displacement is monitored by a linear variable differential transformer (LVDT) and the measured lag between the drive signal and the LVDT is the phase angle. The phase angle and drive signal are used to calculate the elastic modulus E' and damping capacity E'' of the specimen [15]. In the case of the short fiber-reinforced composites, the samples were cut so that the $4 \times 55\,mm^2$ area was oriented parallel to the plane of random fiber orientation. The Young's modulus of the specimens was measured as a function of temperature using a heating rate of 3 K/min from room temperature (RT) to 300°C. At higher temperatures (>350°C), the energy loss component increases considerably due to plastic deformation in the sample, giving erroneous values of Young's modulus. The specimens were clamped and then subjected to a uniform sinusoidal displacement of constant maximum amplitude of 40 μm. The oscillation frequency was fixed at 1 Hz. Two samples or more for each material were tested in

order to check the reproducibility of results, showing identical results for each material in both AC and ST conditions.

In the case of Al99.5/SiC/70p and AlSi7Mg/SiC/70p composites, the Young's modulus has been determined by means of Elastotron 2000™ at the Institute of Physics at the University of Vienna (by Puchegger et al. [16]). This is achieved by free vibrating long thin specimens of rectangular cross section ($5 \times 4.8 \times 60\,mm^3$) supported by carbon fibers [17]. The specimen hangs between graphite heating elements in a vacuum chamber. The experimentally measured set of resonant frequencies is precisely obtained by finding the roots of the derivative response signal of the receiver and then compared with predictions from theory based on Timoshenko's equation. The accuracy of this method is around 1–2%.

THEORETICAL ESTIMATIONS OF THE YOUNG'S MODULUS OF TWO-PHASE COMPOSITES

The modeling of Young's modulus of composite materials has been estimated by means of several theoretical estimations, which depend on the morphological arrangement of materials components. The models were applied following the subsequent considerations: For the case of the Al–Si alloys the reinforcement phase was Si and the matrix phase was Al. For the SFRMs, the reinforcement phase was the Al_2O_3 fibers, and the matrix phase was the composite alloy (AlSi1, AlSi7, AlSi12, and AlSi18) in the corresponding thermal condition (AC or ST). In case of the PRMs, the reinforcement phase was SiC and the composite alloy for the matrix (Al99.5, AlSi7, AlSi7Mg) also in the corresponding thermal condition (AC or ST).

The volume fraction of the Si phase in Al–Si alloys is calculated by subtracting the maximum dissolved Si fraction at the eutectic temperature (1.7 wt%) from the nominal Si content. For the case of the short fiber composites and 10 vol% composites, the Young's modulus was calculated using the experimental data of the unreinforced matrices presented in this work. Tables 2 and 3 summarize the input data for the different models (physical constants and volume fraction of the different phases, respectively).

Rule of Mixtures

For the purpose of comparison, the well-known rule of mixtures (ROM) was used in this work for estimating the Young's moduli of the composites as if they were composed of two slabs bonded together [18]. In case of normal stress being applied parallel to the slab direction (equally strained phases), a weighted mean between the moduli of the two components is obtained (ROM Voigt model [18]):

$$E_C = E_m V_m + E_r V_r, \tag{1}$$

where E and V are the Young's modulus and the volume fraction of the material components, and the subscripts m and r represent the matrix and reinforcing phases, respectively. The prediction of the transverse stiffness (equally stressed phases) gives the lower bound which is often described as the ROM Reuss model [18]:

$$E_C = \left[\frac{V_r}{E_r} + \frac{V_m}{E_m}\right]^{-1}. \tag{2}$$

Table 2. Physical constants for the modeling of Young's moduli of alloys and composites.

Component	Young's modulus (GPa)	Poisson ratio
Al	69 [26]	0.33 [26]
AlSi7Mg	74 [14]	0.33 [14]
Si	162 [26]	0.22 [26]
SiC	450 [26]	0.22 [26]
Al_2O_3	370 [27]	0.22 [27]
AlSi7[a]	74 (AC)/72 (ST)	0.33
AlSi12[a]	77 (AC)/75 (ST)	0.33
AlSi18[a]	84 (AC)/82.5 (ST)	0.33

[a]Obtained experimentally in this work.

Table 3. Microstructural parameters for modeling of the Young's modulus.

Material	Matrix/volume fraction (%)	Reinforcement/volume fraction (%)
AlSi1	Al/100	Si/0
AlSi7	Al/92	Si/6.2
AlSi12	Al/82.3	Si/11.9
AlSi18	Al/79.7	Si/18.5
AlSiX/Al_2O_3/20s	AlSiX/80	Al_2O_3/20[b]
AlSi7Mg/SiC/10p	AlSi7Mg/90	10
Al99.5/SiC/70p	Al99.5/30	70
AlSi7Mg/SiC/70p	AlSi7Mg/30	70
Al_2O_3 short fibers[a]: $r_0 = 2\,\mu m$, $L = 68\,\mu m$, aspect ratio $s = 34$		

[a]From microstructural quantification only for shear-lag estimation; [b]in case of shear-lag estimation the effective volume fraction of short fibers was estimated by using correction factor of 2/5 (Effective vol. fraction = 8% = 20% × 2/5) [24].

Hashin–Shtrikman

The Hashin–Shtrikman (HS) bounds [19] refer to isolated spherical inclusions coated by a second phase. For this estimation no inclusion–inclusion interaction among neighboring inclusions is considered. The upper HS bound is then analogous to the case in which the softer phase is the inclusion material, while the lower bound is equivalent to the case in which the stiffer phase is the inclusion material. The HS lower bound can be calculated as [10]:

$$E_C = \frac{E_m[E_m V_m + E_r(V_r + 1)]}{E_r V_m + E_m(V_r + 1)}. \tag{3}$$

Tuchinskii Model

This section was originally written by Moon et al. [11]. The Tuchinskii model [12] considers a two-phase interpenetrating skeletal structure, where a cube of height 'H' is composed of a skeletal structure of phase 1, the cavity of which is filled with phase 2 of a characteristic dimension h [11]. A repeating array of unit cubes thus forms an interpenetrating skeletal structure for both phases. The ratio of the lengths, $c = h/H$,

can be related to the volume fraction of each phase, $V_m + V_r = 1$, by the following relationship:

$$V_m = (3 - 2c)c^2. \tag{4}$$

The effective composite Young's modulus is calculated in two steps. First, a unit cell is sectioned, either parallel or perpendicular to the loading direction, into three volume elements, each having their own effective Young's modulus, as calculated using either the iso-stress or iso-strain ROM models. Secondly, the volume elements are 'reassembled' and the effective composite Young's modulus of the unit cube is then calculated by using the ROM with the effective Young's moduli of each layer. The Tuchinskii upper bound is calculated by initially sectioning perpendicular to the loading direction and using the ROM Voigt estimation in the final step, while the lower bound is calculated by initially sectioning parallel to the loading direction and using the ROM Reuss equation in the final step. The Tuchinskii upper (+) and lower (−) bounds are given by the following equations:

$$E_C(+) = E_r\left[\frac{1-c}{(1-c^2)+(E_m/E_r)c^2} + \frac{c}{(1-c)^2+(E_m/E_r)(2-c)c}\right]^{-1}, \tag{5}$$

$$E_C(-) = E_r\left[(1-c)^2 + (E_m/E_r)c^2 + \frac{2(E_m/E_r)c(1-c)}{c+(E_m/E_r)(1-c)}\right]. \tag{6}$$

Shear Lag

The most widely used model describing the effect of loading for aligned short fiber composites is the so-called shear-lag model, originally proposed by Cox [20] and afterwards developed by others [21–23]. This model is based on the transfer of tensile stress from the matrix to the fibers by means of interfacial shear stresses. The basis of these calculations is well described in [18], where a comprehensive mathematical treatment is given. The external loading is applied parallel to the fiber axis. The model is based on considering the radial variation of shear stress in the matrix and at the interface. In this way, the axial Young's modulus of the composite E_{3C} can be expressed as:

$$E_{3C} = \left\{V_r E_r\left[1 - \frac{\tan \mathrm{h}(ns)}{ns}\right] + V_m E_m\right\}, \tag{7}$$

where n is a dimensionless constant given by:

$$n = \left[\frac{2E_m}{E_r(1+\nu_m)\ln(1/V_r)}\right]^{1/2}, \tag{8}$$

and s is the fiber aspect ratio L/r_0, L and r_0 are the fibers' length and radius, respectively, and ν_m is the Poisson's ratio of the matrix.

The present model is only used in this work for predicting the Young's Modulus of the short fiber materials. Since the SFRMs present a random planar distribution of the fibers and the present model is based of simple aligned fiber to test direction, the effective volume fraction of the reinforcing phase must be corrected. Therefore, a correction factor of 2/5 was applied in order to estimate the effective volume fraction of fibers as proposed by Dlouhy et al. [24]. Finally, the corrected volume fraction is presented in Table 3.

MORPHOLOGICAL ANALYSIS

The 2D metallographies of the unreinforced AlSi7, AlSi12, and AlSi18 alloys in the as cast condition and of the AlSi12 after ST condition, are depicted in Figure 1(a)–(d). Both the AlSi7 and AlSi12 alloys behave hypoeutectically, showing the primary α-phase enclosed by the eutectic Al–Si phase, and amounting to ~75 and 25 vol%, respectively (these values were obtained after analyzing several low magnification metallographies, while only the eutectic structure is observed in the figures). The AlSi12 alloys shows a few primary Si particles of <0.1 vol% owing to the nonequilibrium cooling conditions experienced by the squeeze casting process. The interconnected Si lamellae present a large surface/volume ratio in 3D for all investigated as cast alloys [25]. On the other hand, the lamellar structure disintegrates and coarsens into rounded Si particles [2] after heating at 540°C for 4 h (ST condition). A continuous Si network is observed after leaching of the Al-phase in all the AlSi alloys in the as cast condition (e.g., AlSi7; Figure 1(e)). The AlSi18 alloy presents mostly a eutectic composition and relatively large primary Si particles of around 5 vol%. Although this last alloy represents a hypereutectic composition, less than 1 vol% of primary α-phase was recorded in the alloy. A primary Si particle of around 60 μm is depicted in Figure 1(f) after leaching of the Al-phase, from which several Si lamellae emanate with no preferential orientation. The interpenetrating Si networks in the as cast condition are very sensitive to solution treatment, disintegrating when heated

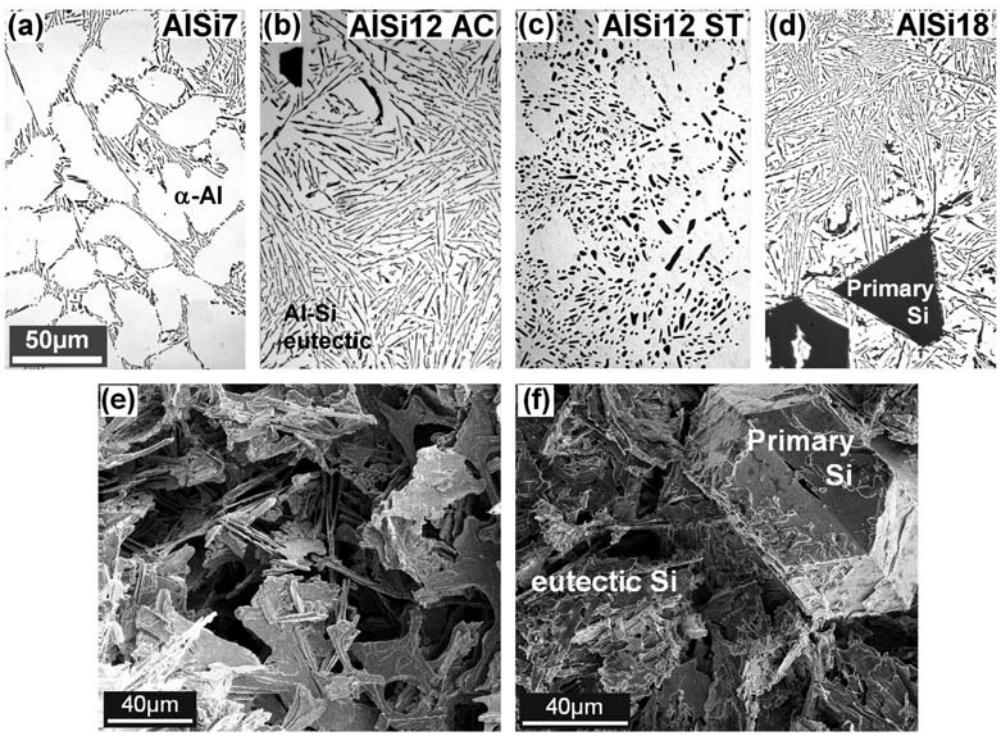

Figure 1. *(a) Light Optical Micrographs (LOM) of the (a) AlSi7, (b) AlSi12, and (d) AlSi18 alloys in the as cast condition (AC) and (c) after spheroidization treatment (ST) in the AlSi12 (white: Al, dark: Si); as cast self-supporting Si networks obtained after leaching of the Al-phase from (e) AlSi7 and (f) AlSi18.*

at 540°C. Coarse and isolated Si particles were observed after 20 min of exposure time at 540°C [25].

The SFRMs present an in-plane random distribution of the Al_2O_3 fibers perpendicular to the infiltration plane (Figure 2(a)). The AlSi1.1/Al_2O_3/20s matrix shows only primary α-phase since the Si content is too low to form a eutectic. The microstructure of the composites' matrices is similar to that of the unreinforced alloys, but the width of the α-dendrites enclosed by the eutectic structure is significantly smaller in AlSi7/Al_2O_3/20s (Figure 2(a)). The eutectic is concentrated around fibers indicating that solidification started at these places. About 15 vol% primary α-phase can be observed between the eutectic for the AlSi12/Al_2O_3/20s composite (Figure 2(c)). The AlSi18/Al_2O_3/20s composite (Figure 2(d)) shows mostly a eutectic microstructure with ~3 vol% of primary Si particles, but as well as primary α-phase dendrites. Interconnected hybrid Si–Al_2O_3 structures are observed after leaching of the Al-phase. Here interconnected networks of the eutectic Si itself as well as of Si eutectic-plates bridging the Al_2O_3 fibers are observed (Figure 2(e)). During ST treatment, the Si plates coarsened into Si-particles, reducing the number of Si bridges. The Si particles sticking to the Al_2O_3 fibers are shown in Figure 2(f) (AlSi12/Al_2O_3/20s). Most of the Si particles become disconnected and are lost during leaching. The number of Si bridges is significantly reduced. The reinforced AlSi18

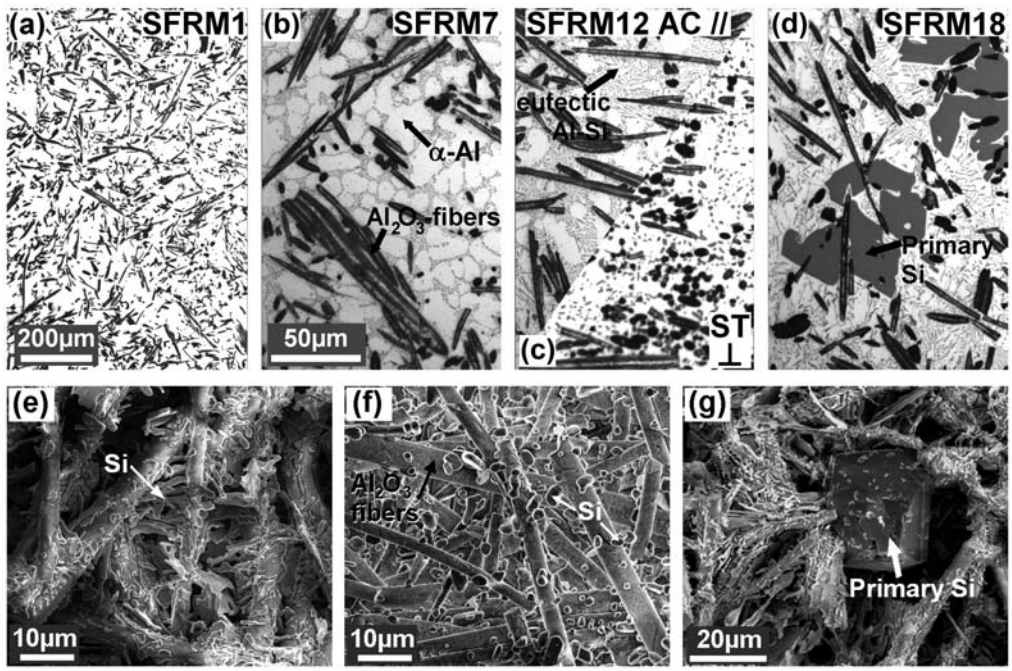

Figure 2. *LOM micrographs of the different short fiber reinforced composites showing (a) the planar random distribution of the fibers in SFRM1; higher magnification of eutectic structures in reinforced (b) AlSi7 (c) AlSi12 in fiber plane and perpendicular planes; and (d) AlSi18 alloys (eutectic microstructure after ST treatment in SFRM12 perpendicular to fiber plane is presented in (c); self-supporting Si–Al_2O_3 networks obtained after leaching the α-Al phase from AlSi12/Al_2O_3/20s in (e) as cast and (f) after ST; (g) AlSi18/Al_2O_3/20s in the as cast condition showing primary Si particles.*

matrix contains eutectic Si and also primary Si particles of about $10^4\,\mu m^3$ interconnecting the alumina fibers (Figure 2(g)). The connectivity between the primary Si and the fibers is conserved even in ST condition.

In AlSi7Mg/SiC/70p and Al99.5/SiC/70p (Figure 3(a)) composites, SiC particles of trimodal size distribution are densely packed. After the dendritic solidification of the primary α-phase of the AlSi7Mg matrix, the remaining eutectic liquid (containing 12.6 wt% Si) tends to solidify around the particles. The SEM micrograph (Figure 3(b)) of AlSi7Mg/SiC/70p, where the primary α-phase has been leached off, visualizes the Si-bridges between the SiC particles forming a percolating SiC–Si network [14]. Of course, such Si bridges do not exist in Al99.5/SiC/70p composite formed by pure Al-matrix, where the SiC particles fall apart after removal of the Al-phase. The AlSi7/SiC/10p composite presents a homogenous distribution of the SiC particles (Figure 3(c)) of ~37 μm in diameter. Particle free zones (regions in the Al-matrix which are free of SiC particles) of around 6 vol% are observed. The eutectic Si structure solidifies at the SiC particles forming a continuous network of SiC particles connected by eutectic Si connected structure (Figure 3(d)). This hybrid network is disintegrated immediately when heated to 540°C, where Si disintegrates into isolated particles.

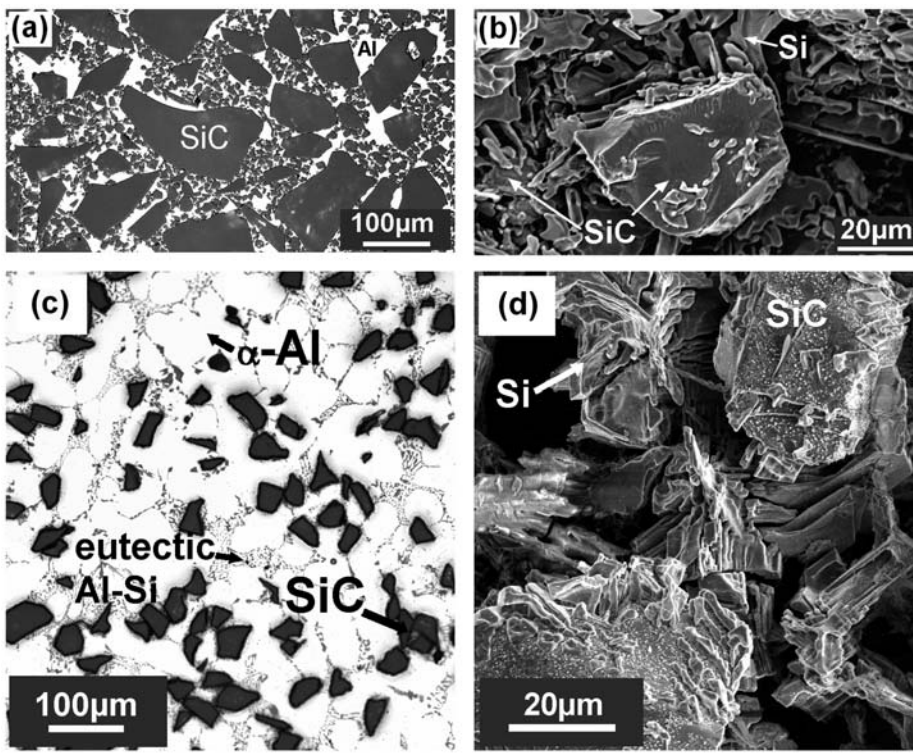

Figure 3. *Light optical micrographs of (a) Al99.5/SiC/70p composite showing a trimodal distribution of the SiC particles and (c) AlSi7/SiC/10p. Porous structure obtained after leaching of the α-phase from (b) AlSi7Mg/SiC/70p and (d) AlSi7/SiC/10p composites.*

RESULTS OF YOUNG'S MODULUS DETERMINATIONS

Figure 4 and Table 4 show the experimental results for the Young's Modulus of the studied matrices and composites at temperatures between 25°C and 300°C. The Young's modulus of the alloys increases with the Si content. The hypereutectic AlSi18 alloy in the as cast condition presents significantly higher *E*-values over the entire investigated temperature range compared to the other unreinforced alloys. The Young's modulus was 84 GPa at RT and decreased to 71 GPa at 300°C (~15% lower). The recorded values

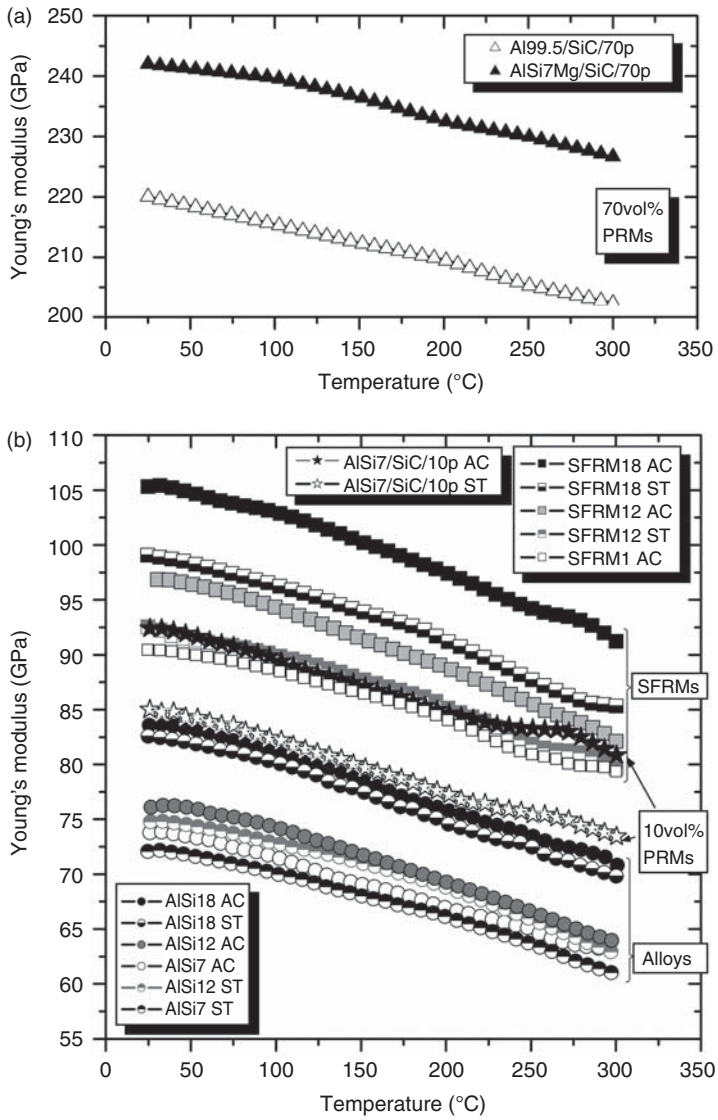

Figure 4. *Values of Young's modulus vs. temperature for (a) the AlSi7, 12 and 18 alloys, AlSi1-12-18/Al_2O_3/20s composites for stresses applied in the fiber plane, and AlSi7/SiC/10p in the as cast condition and after 540°C/4 h (ST); (b) Al99.5/SiC/70p and AlSi7Mg/SiC/70p composites.*

for the hypoeutectic AlSi12 and AlSi7 in the as cast condition were 77 and 74 GPa at RT, respectively. After ST treatment, a slight reduction in the Young's moduli to 75 and 72 GPa, respectively (~2% lower), was observed for the AlSi12 and AlSi7 alloys, and 82.5 (1.7% lower with respect to AC) for AlSi18 in the ST condition.

The stiffness of the unreinforced matrices was increased by ~25% by the addition of 20 vol% Al_2O_3 fibers. The Young's modulus of AlSi18/Al_2O_3/20s in the as cast condition was the highest amounting to 106 and 91 GPa at RT and 300°C, respectively. In the case of AlSi12/Al_2O_3/20s and AlSi1/Al_2O_3/20s, values of 97–82 GPa, and 91–79 GPa are observed from RT to 300°C, respectively. Similar to the unreinforced alloys, the Young's moduli of the materials decreased in the ST condition by ~5–6% for SFRM18 (99 GPa) and SFRM12 (92 GPa) at RT, being around 20% higher than that of the unreinforced Al–Si alloys. On the other hand, AlSi1/Al_2O_3/20s exhibited the same Young's moduli in the as cast condition and after ST treatment, with values of 91 and 80 GPa at RT and 300°C, respectively.

The addition of 10 vol% SiC particles increased the *E*-values of the AlSi7 by ~25%, amounting to 92 GPa at 25°C to 81 GPa at 300°C. As observed before, the spheroidization of the Si lamellae decreased the stiffness (by ~8%) of the composite to 85 and 73 GPa at RT and 300°C, respectively.

DISCUSSION

For the purpose of comparison and interpretation, different elastic models have been applied to predict the Young's modulus of multi-phase materials. The resulting alloy and composite moduli are influenced by the phase morphology, particularly the continuity of the stiffest phase, stiffness difference of the constituents and the volume fraction of each phase.

Table 4. Experimental Young's modulus and theoretical predictions (GPa).

		Theoretical predictions (at RT)			
Sample name	**Experimental SD: ± 1% (RT/300°C)**	**ROM (Reuss/Voight)**	**HS (–)**	**Tuchiniskii (+)/(–)**	**Shear lag**
AlSi7 AC	74/63	71.6/74.8	72.7	73.0/74.0	(–)
AlSi7 ST	72/61				
AlSi12 AC	77/65	74.2/80.0	76.0	76.7/78.4	(–)
AlSi12 ST	75/63				
AlSi18 AC	84/71	77.3/86.0	80.1	81.2/83.4	(–)
AlSi18 ST	82.5/70				
AlSi7/SiC/10p AC	92/81	80.5/111.4	85.2	92.7/(–)	(–)
AlSi7/SiC/10p ST	85/73	79/110.2	83.7	91.3/(–)	(–)
Al99.5/SiC/70p	220/(–)	169.8/335.9	215.4	260.6/(–)	(–)
AlSi7Mg/SiC/70p	242/(–)	175.9/336.8	220.7	264.0/(–)	(–)
AlSi1/Al_2O_3/20s AC	91/79	82.6/(–)	(–)	(–)	90.6
AlSi1/Al_2O_3/20s ST	91/79	82.6/(–)	(–)	(–)	90.6
AlSi12/Al_2O_3/20s AC	97/82	90.8/(–)	(–)	(–)	97.3
AlSi12/Al_2O_3/20s ST	92/80	88.9/(–)	(–)	(–)	95.9
AlSi18/Al_2O_3/20s AC	106/91	98.8/(–)	(–)	(–)	104.0
AlSi18/Al_2O_3/20s ST	99/85		(–)	(–)	103.1

The appropriateness of the various models for predicting Young's modulus will depend on each of the above-narrated issues. The HS lower bound is considered to be appropriate to isolated spherical inclusions coated by a second phase. The Tuchinskii estimation considers interpenetrating structures of the reinforcement, but uses a simplified unit cell. The upper and lower bounds of the ROM (Voigt and Reuss, respectively) refer to the volume fraction of the phases without interaction and are given for comparison. The results from the theoretical predictions are summarized and compared with the experimental results in Table 4.

The experimental and estimated Young's moduli vs. Si eutectic content for the Al–Si alloys (at RT) are depicted in Figure 5. In general, the as cast condition of the different Al–Si alloys is well represented by the Tuchinskii upper bound, where the eutectic Si lamellae and the relatively large primary Si inclusions (in AlSi18) form an interconnected porous structure which increases the Young's modulus of the alloy. The Young's modulus of the ST samples (containing isolated Si particles) decreases below the HS (−) estimation for particles without connectivity. The experimental result of the AlSi12 alloy in AC falls down to the Tuchinskii lower bound, but presenting also an enhanced Younǵs modulus with respect to the ST version.

Figure 6(b) shows the experimental results for the two 70 vol% particle reinforced Al99.5 and AlSi7Mg matrices and their theoretical composite predictions for the corresponding matrix. The Young's modulus of Al99.5/SiC/70p was 220 GPa, while for AlSi7Mg/SiC/70p it was 10% higher (242 GPa). This difference cannot be solely attributed to differences in matrix stiffness since the Young's modulus of AlSi7Mg is only ~5 GPa higher than that of pure-Al. It is believed that the interconnected structure results in the increase of the measured Young's modulus. Supporting this is the observation of a self-supporting interconnected SiC–Si structure after leaching of the Al-phase for the AlSi7Mg/SiC/70p composite, where the Si lamellae connect the SiC particles (Figure 3(b)). This was not observed for the Al99.5/SiC/70p composite in which its

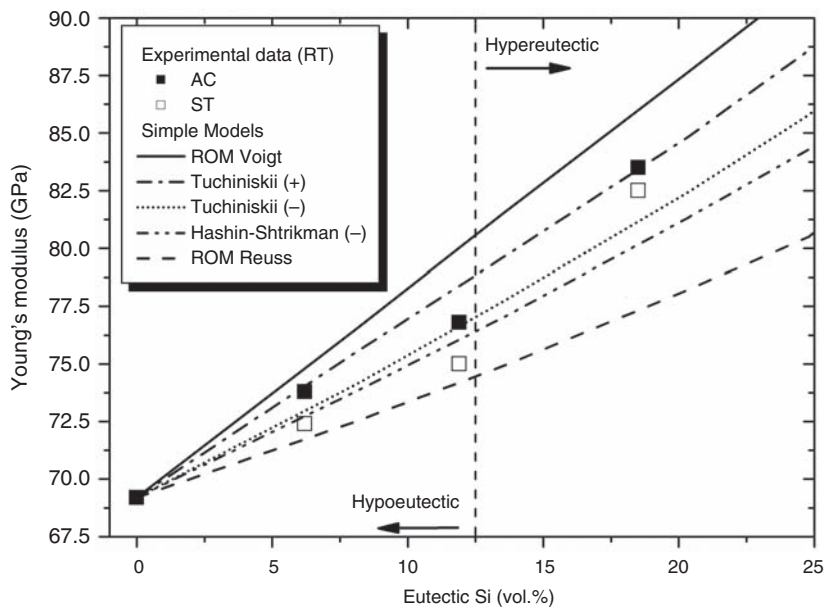

Figure 5. *Modeled and experimental Young's moduli at RT for pure-Al and the different Al–Si alloys.*

structure is completely disintegrated during the leaching process. Since the Si content tends to solidify around the SiC particles in AlSi7Mg/SiC/70p (due to the large volume content of the reinforcing phase), a spheroidization treatment does not reduce connectivity, and therefore the Young's modulus.

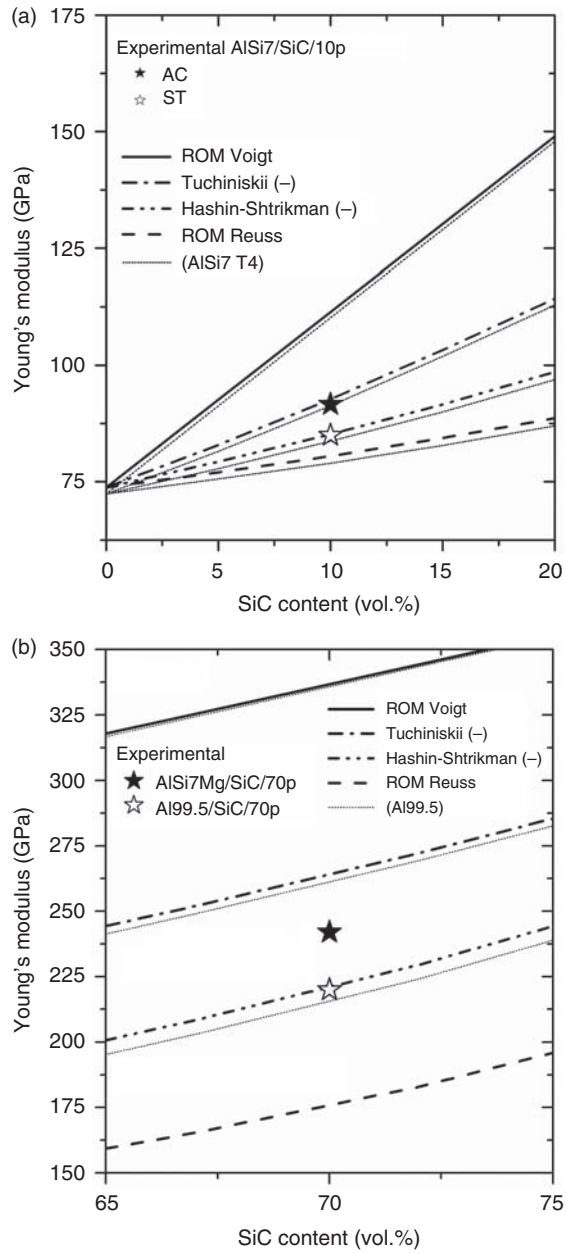

Figure 6. *Experimental and estimated values of the effective Young's modulus in (a) AlSi7/SiC/10p in the as cast condition and after spheroidization treatment (dash line) and (b) Al99.5/SiC/70p and AlSi7Mg/SiC/70p composites (estimations using Al99.5 matrix are represented in dash line).*

The discontinuous reinforcement phase in Al99.5/SiC/70p composite is similar to the HS model, which considers discontinuous spherical inclusions, and thus it predicts the Young's modulus of this composite as demonstrated in Figure 6(b). In contrast, AlSi7Mg/SiC/70p composite has the interconnected structure which increases the Young's modulus near to that predicted by Tuchinskii lower bound for interpenetrating structures. Similarly, the Young's modulus of the hybrid Si–SiC structure observed for the as cast AlSi7/SiC/10p composite is well estimated by the Tuchinskii lower bound (Figure 6(a)). The disintegration of the network during spheroidization treatment decreases the stiffness of the material by ~8%, falling to the HS lower bound estimation.

Figure 7 depicts the experimental values, along with the shear lag and ROM Reuss predictions of the Young's modulus vs. the Si content for the different SFRMs. Here, the Young's modulus is modeled for both theoretical predictions using the experimental matrix results of AC and ST conditions. A good agreement between the experimental results and the shear-lag model is observed for materials tested in the AC condition. From the experimental results, the Young's modulus of AC conditions increases by 0.4 GPa/eutectic Si vol% up to the eutectic composition (~12.5 vol%) and increases above the eutectic compositions by 1.6 GPa/eutectic Si vol% for the hypereutectic compositions. Note that both the shear-lag and ROM Reuss estimations predict a higher slope between Si 0 and 6 vol% than for 6 and 12 vol% in the hypoteutectic range, while it is constant in the ST samples (between Si 0 and 12 vol%). The connectivity of the Si phase in AC AlSi7 matrix may be responsible for this effect compared with the almost pure Al and ST matrices. Further investigations in materials with intermediary Si compositions must be carried out to confirm this observation. For the case of the hypereutectic composition, the addition of the primary Si particles connecting several Al_2O_3 fibers is considered to be responsible for the higher slope in both AC and ST conditions. While in SFRM12 the

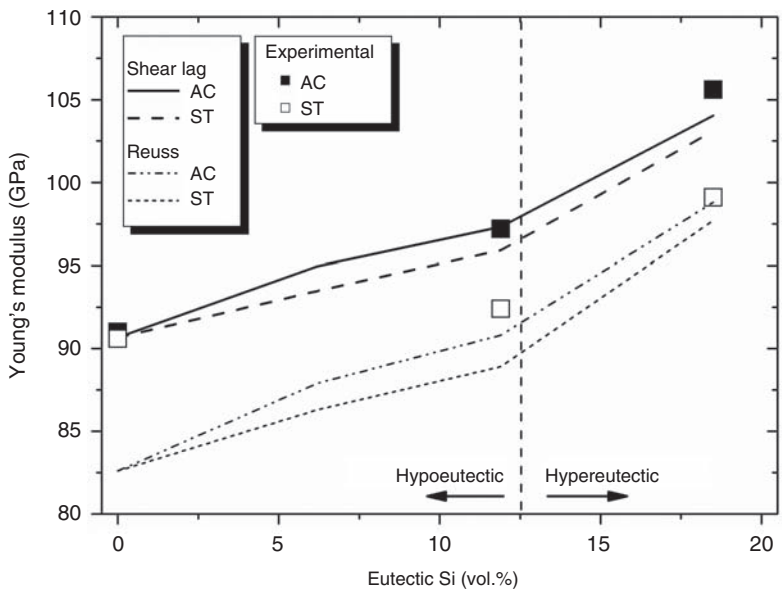

Figure 7. *Experimental and estimated values (shear lag + Reuss model) of the Young's modulus in AlSiX/Al_2O_3/20s (X = 1, 7*, 12, 18); *only theoretical predictions.*

solution treatment decreases the Young's moduls to the level of the almost non-Si containing SFRM, the *E*-value for SFRM18 in ST is still higher than SFRM12 in AC. This may be attributed to the large Si particles connecting the fibers in the hypereutectic composite. Of course, the observed higher *E*-values with increasing Si content is not only a consequence of connectivity, but also a result of the addition of the stiffer Si phase (with respect to Al).

A decreasing Young's modulus is observed in the SFRMs with Si content >12 wt% after ST treatment, dropping even below the shear-lag estimation (with ST matrices). The shear-lag model predicts a difference of only 1.5 and 2 GPa in stiffness for SFRM12 and SFRM18, respectively, using the matrix values with interpenetrating (AC) and isolated (ST) structures. On the other hand, a reduction of around 5 and 7 GPa was recorded experimentally for both SFRM12 and SFRM18 composites, respectively, while for the case of unreinforced AlSi12 and AlSi18 alloys, this difference amounts only around 1.5–2 GPa. The ripening of the Si lamellae decreases the connectivity of the Si–Al_2O_3 hybrid network in the composite materials, thus reducing the effectiveness of the reinforcement and suggesting a strong interaction between the Al_2O_3 fibers and the Si structure.

CONCLUSIONS

Unreinforced and reinforced Al–Si alloys (containing 25 vol% or more Al–Si eutectic) present interconnected Si structures after fast solidification (AC conditions). Hypoeutectic Al–Si alloys show a continuous Si network composed of thin interconnected Si lamellae [25] which contribute to the stiffness of the alloys. For the case of hypereutectic compositions, this network is also composed of relatively large primary Si particles. The difference is revealed after spheroidization of the Si phase by a solution treatment owing to the disintegration of the Si network by decreasing slightly the elastic modulus of the unreinforced AlSi alloys.

The addition of Al_2O_3 short fibers or SiC particles to the Al–Si matrices enhances the formation of a continuous rigid structure composed of Si–Al_2O_3 and Si–SiC networks in the as cast conditions, which improves the Young's modulus considerably. The effect of the interconnected reinforcement is enhanced for composite materials, where the disintegration of the Si–Al_2O_3 and Si–SiC structures by a solution treatment decreases the Young's modulus. On the other hand, the Young's modulus of AlSi1.1, AlSi1/Al_2O_3/20s, and Al99.5/SiC/70p materials does not change by a ST treatment, since the Si content is too low to form a eutectic network.

The Tuchinskii and HS lower bound predicts the effect of the morphological changes on the materials properties. The experimental results for the unreinforced Al–Si and the PRMs with interpenetrating structures are well estimated by the Tuchinskii equation, while the HS lower bound is in agreement with the experimental results for the ST or Si free PRMs (no-continuous structures). In the case of the ST Al–Si alloys, the Young's modulus agrees with the ROM Reuss estimation.

A good approximation of the effective Young's modulus in the fiber plane is obtained from the shear-lag model for the SFRMs. A difference of only ~1.5% between ST and AC conditions was predicted, while it was more than 5% experimentally in SFRM7 and SFRM12. The shear-lag model should be extended to the Si-bridges connecting the fibers in the as cast condition.

ACKNOWLEDGMENTS

The authors would like to thank Dr Thomas Huber for metallographic observation and Young's modulus estimation of the 70 vol% SiC composites, as well as Martín Duarte and Enrique Louis of the Alicante University for providing the AlSi7/SiC/10p samples. F. Lasagni is grateful to funding by ARC Leichtmetallkompetenzzentrum Ranshofen GmbH (Austria) via the Austrian Non-Kplus-programme.

REFERENCES

1. Lasagni, F., Lasagni, A., Holzapfel, C., Mücklich, F. and Degischer, H.P. (2006). Three Dimensional Characterization of Unmodified and Sr-Modified Al-Si Eutectics by FIB and FIB EDX Tomography, *Advanced Engineering Materials*, **8**(8): 719–723.
2. Lasagni, F., Degischer, H.P. and Papakyriacou, M. (2006). Influence of Solution Treatment, Sr-Modification and Short Fiber Reinforcement on the Eutectic Morphology of Al-Si Alloys, *Praktische Metallographie*, **43**(6): 271–285.
3. Kelly, A. and Zweben, C. (2000). *Comprehensive Composite Materials*, Vol. 3, Elsevier Science Ltd, Oxford.
4. Requena, G. and Degischer, H.P. (2004). Creep Behaviour of Unreinforced and Short Fiber Reinforced AlSi12CuMgNi Piston Alloy, *Materials Science and Engineering: A*, **420**(1–2): 265–275.
5. Schnabl, A. and Degischer, H.P. (2003). Thermal Cycling Creep of a Short Fiber Reinforced Aluminium Piston Alloy, *Zeitschrift für Metallkunde*, **94**(6): 743–748.
6. Kouzeli, M. and Dunand, D.C. (2003). Effect of Reinforcement Connectivity on the Elasto-Plastic Behavior of Aluminum Composites Containing Sub-Micron Alumina Particles, *Acta Materialia*, **51**(20): 6105–6121.
7. Peng, H.X., Fan, Z. and Evans, J.R.G. (2001). Bi-Continuous Metal Matrix Composites, *Materials Science and Engineering A*, **303**(1–2): 37–45.
8. Wegner, L.D. and Gibson, L.J. (2000). The Mechanical Behaviour of Interpenetrating Phase Composites – I: Modelling, *International Journal of Mechanical Sciences*, **42**(5): 925–942.
9. Peng, H.X., Fan, Z. and Evans, J.R.G. (2001). Bi-continuous Metal Matrix Composites, *Materials Science and Engineering A*, **303**: 37–45.
10. Ibrahim, I.A., Mohamed, F.A. and Lavernia, E.J. (1991). Particulate Reinforced. Metal Matrix Composites-a Review, *Journal of Materials Science*, **26**: 1137–1156.
11. Moon, R.J., Tilbrook, M., Hoffman, M. and Neubrand, A. (2005). Al-Al2O3 Composites with Interpenetrating Network Structures: Composite Modulus Estimation, *Journal of the American Ceramic Society*, **88**(3): 666–674.
12. Tuchinskii, L.I. (1983). Elastic Constants of Pseudoalloys with a Skeletal Structure, *Metallurgiya*, **247**(7): 85–92 (Translated in *Powder Metallurgy and Metal Ceramics*, **85**: 588–595).
13. Torquato, S., Yeong, C.L.Y., Rintoul, M.D., Milius, D.L. and Aksay, I.A. (1999). Elastic Properties and Structure of Interpenetrating Boron Carbide/Aluminum Multiphase Composites, *Journal of the American Ceramic Society*, **85**(5): 1263–1268.
14. Huber, T., Degischer, H.P., Lefranc, G. and Schmitt, T. (2006). Thermal Expansion Studies on Aluminium-Matrix Composites with Different Reinforcement Architecture of SiC Particles, *Composites Science and Technology*, **66**(13): 2206–2217.
15. Elomari, S., Boukhili, R., Skibo, M.D. and Masounave, J. (1995). Dynamic Mechanical Analysis of prestrained Al_2O_3/Al Metal-Matrix Composite, *Journal of Materials Science*, **30**(12): 3037–3044.
16. Puchegger, S., Loidl, D., Kromp, K. and Peterlik, H. (2003). In: Degischer, H.P. (ed), *Proceedings 14. Symposium–Verbundwerkstoffe und Werkstoffverbunde 2003*, Wiley-VCH, Weinheim, pp. 280–285.

17. Kaindl, G., Lins, W., Peterlik, H., Kromp, K., Reetz, R. and Reetz, T. (2000). The Determination of the Elastic Moduli of Anisotropic Ceramics and Ceramic Composites at High Temperatures by a Novel Resonant Beam Technique, *Interceram*, **49**(2): 92–101.
18. Clyne, T.W. and Withers, P.J. (1993). *An Introduction to Metal Matrix Composites*, Cambridge University Press, London, UK.
19. Hashin, Z. and Shtrikman, S. (1963). A Variational Approach to the Theory of the Elastic Behaviour of Multiphase Materials, *Journal of Mechanics and Physics of Solids*, **11**: 127–140.
20. Cox, H.L. (1952). The Elasticity and Strength of Paper and Other Fibrous Materials, *British Journal of Applied Physics*, **3**: 73–79.
21. Outwater, J.O. (1956). The Mechanics of Plastics Reinforced in Tension, *Modern Plastics*, **33**: 56–65.
22. Rosen, B.W. (1965). *Mechanics of Fiber Strengthening, in Fiber Composite Materials*, American Society for Metals, Metals Park, Ohio.
23. Dow, N.F. (1963). *Study of Stresses Near Discontinuity in a Filament – Reinforced Composite Metal*, GE Co., Missile and Space Div., R635D61.
24. Dlouhy, A., Eggeler, G. and Merk, N. (1995). A Micromechanical Model for Creep in Short Fiber Reinforced Aluminium Alloys, *Acta Metallurgica et Materialia*, **43**(2): 535–550.
25. Lasagni, F., Lasagni, A., Holzapfel, C., Mücklich, F. and Degischer, H.P. (2007). Three-Dimensional Characterization of 'As-Cast' and Solution-Treated AlSi12(Sr) Alloys by High-Resolution FIB Tomography, *Acta Materialia*, **55**(11): 3875–3882.
26. Bauccio, M. (ed.) (1994). *ASM Engineered Materials Reference Book*, **2nd edn**, ASM International, Materials Park, OH.
27. King, J.A. (1998). *Materials Handbook for Hybrid Microelectronics*, Artech House, Nordwood, MA.